**SUPPLEMENTARY INFORMATION**

**SI FIGURES**

**SI Fig. 1. Decreased miR-9 levels occur in SZ NPCs but not SZ hiPSC forebrain neurons, presented by individual, related to Figure 1.**

**A-D.** Experimental replicates, by NPC line and experimental replication, of the qPCR validation of normalized miR-9 expression during the differentiation of SZ NPCs (**A**) into 1- (**B**), 2- (**C**) and 6-week-old (**D**) neurons. **E.** qPCR of normalized miR-9 expression in post-mortem DLPFC tissue from ten SZ patients and ten controls. Error bars are s.e., *P < 0.05, **P < 0.01, ***P < 0.001.

**SI Fig. 2. Validation of COS hiPSCs and NPCs, related to Figure 1.**

**A.** RT-PCR gels showing that hiPSCs derived from both control (C) and childhood-onset-SZ (COS) patient (P) fibroblasts expressed the human pluripotency markers *cMYC*, *OCT4*, *NANOG* and *LIN-28*. RT-PCR results from validated BJ (ATCC CRL-2522) hiPSCs and a control fibroblast cell line are also displayed as positive and negative controls, respectively. **B.** Flow cytometry histograms for TRA-1-60 (left panel) and SSEA4 (right panel), black filled trace (control fibroblast cell line), grey trace (control hiPSCs), red trace (COS patient hiPSCs) and blue filled trace (BJ hiPSCs). **C**. A representative karyotype image from a COS patient derived hiPSC line showing no chromosomal abnormalities. **D**. Flow cytometry histograms demonstrating that control (grey) and COS patient (red) hiPSC-derived NPCs express NESTIN (left panel) and SOX2 (right panel).

**SI Fig. 3. Additional top miRNAs and transcription factors with change of activities predicted by the integrative model, related to Figure 2.**

**A-F.** Additional top miRNAs. Scatter plots between expression and predicted change of activities for miRNA-124 (**A**), miR-506 (**B**), miR-218 (**C**), miR-125a (**D**), miR-125b (**E**) and miR-129 (**F**). **G-K.** Top transcription factors. Scatter plots between expression and predicted change of activities for RFX4 (**G**), REST (**H**), IRF1 (**I**), NRF1 (**J**) and HOXA6 (**K**).

**SI Fig. 4. Validation of RV overexpression constructs, related to Figure 3.**

**A-B.** qPCR validation that RV-miR-9 (**A**) and RV-miR-137 (**B**) overexpression in hiPSC forebrain NPCs result in increased miR-9 and miR-137 levels, respectively. **C**. FACS purification of GFP-positive cells from RV-GFP and RV-miR-9 transduced control and SZ NPCs prior to RNAseq analysis. Error bars are s.e., *P < 0.05, **P < 0.01, ***P < 0.001.

**SI Fig. 5. Aberrant migration in SZ hiPSC forebrain NPCs, related to Figure 3.**

**A.** Brightfield images of neurosphere outgrowth in high (Delaloy et al., 2010) and low (Brennand et al., 2014) matrigel conditions, revealing different neurospheres morphologies between the two conditions. **B.** Neurosphere outgrowth by untranduced control and SZ hiPSC forebrain NPCs, in either high or low matrigel conditions. **C.** Neurosphere migration in high matrigel conditions by control and SZ hiPSC NPCs, following transient reduction of miR-9 levels. Migration distance was calculated as the average of the five furthest migrating cells, as in Delaloy *et al*. (2010). Error bars are s.e., *P < 0.05, **P < 0.01, ***P < 0.001.

**SI Fig. 6. Effect of manipulation miR-9 on replication and target gene expression, related to Figures 3 and 4.**

**A.** WST-1 cell viability assay. 24-hour cell viability in control and SZ hiPSC forebrain NPCs, relative to time 0 hour, following stable transduction with RV-GFP, RV-miR-9 or RV-miR137, when assayed by comparing absorbance of WST-1 converted to formazan dye by cellular reductases. **B.** Control and SZ hiPSC forebrain NPCs transduced with RV-GFP, RV-miR-9 or RV-miR137 and stained with the cell cycle marker Ki67 (red). DAPI-stained nuclei (blue). Scale bar 100 μm. **C.** Cell counts for the percentage of GFP-positive control or SZ hiPSC forebrain NPCs, stably transduced with either RV-GFP, RV-miR-9 or RV-miR137, that are positive for the cell cycle protein Ki67 of control and SZ hiPSC forebrain NPCs. **D.** Nanostring nCounter analysis of fold-change of normalized expression of the neural adhesion gene *NRXN1* following stable overexpression of RV-miR-9-GFP, relative to expression in RV-GFP transduced (gray dashed line) control and SZ NPCs. **E.** Nanostring nCounter analysis of fold-change of normalized expression of selected known miR-9 target genes, following stable overexpression of RV-miR-9-GFP,

relative to expression in RV-GFP transduced (gray dashed line) control and SZ NPCs. Error bars are s.e. *P < 0.05, **P < 0.01, ***P < 0.001.

**SI Fig. 7. WGCNA of the "miR-9 perturbation" RNAseq dataset, related to Figure 4.**

**A**. Selection of soft-thresholding powers for WGCNA. The left panel shows the scale-free fit index (y-axis) as a function of the power parameter (x-axis). The right panel displays the mean connectivity (degree, y-axis) as a function of the power parameter (x-axis). **B**. The coexpression network visualization using heatmap, with module assignment and gene dendrogram shown along the left side and the top. Larger gene interaction magnitude is marked by darker colors. Blocks along the diagonal are the modules. As shown in (**A**), the power of 11 shows the best scale-free topology fit. The networks with different powers (10 to 12) were also shown. Consistently, migration-related modules are enriched in all the four networks.

**SI TABLES**

SI Table 1. miRNAs with significant (Benjamini Hochberg-corrected) perturbations in expression in SZ hiPSC NPCs and neurons, related to Tables 1 and 2.

SI Table 2. Raw and normalized miR-9 expression profile in the COS cohort NPCs with the batch effect removed away using a multivariate regression model, related to Figure 1.

SI Table 3. Predictions of miRNAs with perturbed expression in SZ hiPSC NPCs and neurons made from microarray gene expression analysis, related to Tables 1 and 2.

SI Table 4. Significantly differentially expressed genes in SZ hiPSC neurons identified by RNAseq, related to Figure 2.

SI Table 5. Identification of miRNAs with significant activity changes in SZ hiPSC NPCs and neurons, from RNAseq gene expression analysis, related to Figure 2.

SI Table 6. Identification of TFs with significant activity changes in SZ hiPSC NPCs and neurons, from RNAseq gene expression analysis, related to Figure 2.

SI Table 7. Nanostring nCounter analysis of selected miR-9 and miR-137 targets between control and SZ hiPSC NPCs, related to Figure 4.

SI Table 8. Nanostring nCounter analysis of normalized expression of control and SZ hiPSC NPCs, following stable over-expression of RV-miR-9, related to Figure 4.

SI Table 9. Putative direct miR-9 targets revealed by intersecting DE genes between the "SZ NPC signature" and the "miR-9 perturbation" datasets together with complementary information: targetScan and CLIP experiments, related to Figures 4 and 5.

SI Table 10. Putative indirect miR-9 targets revealed by intersecting DE genes between the "SZ NPC signature" and the "miR-9 perturbation" datasets together with complementary LC MS/MS proteomic dataset, related to Figures 4 and 5.

SI Table 11. LC MS/MS quantitative analysis of proteins significantly altered in control or SZ hiPSC NPCs following RV-miR9 overexpression, related to Figure 5.

SI Table 12. DAVID analysis of biological clusters most enriched in control or SZ hiPSC NPCs following RV-miR9 overexpression, related to Figure 5.

SI Table 13. Top 20 enriched gene ontology (GO) terms in putative miR-9 targets from LC MS/MS comparisons of RV-GFP and RV-miR9 overexpressing control and SZ hiPSC NPCs, related to Figure 5.

SI Table 14. Putative miR-9 targets enriched for several migration related gene ontology (GO) terms from LC MS/MS comparisons of RV-GFP and RV-miR9 overexpressing control and SZ hiPSC NPCs, related to Figure 5.

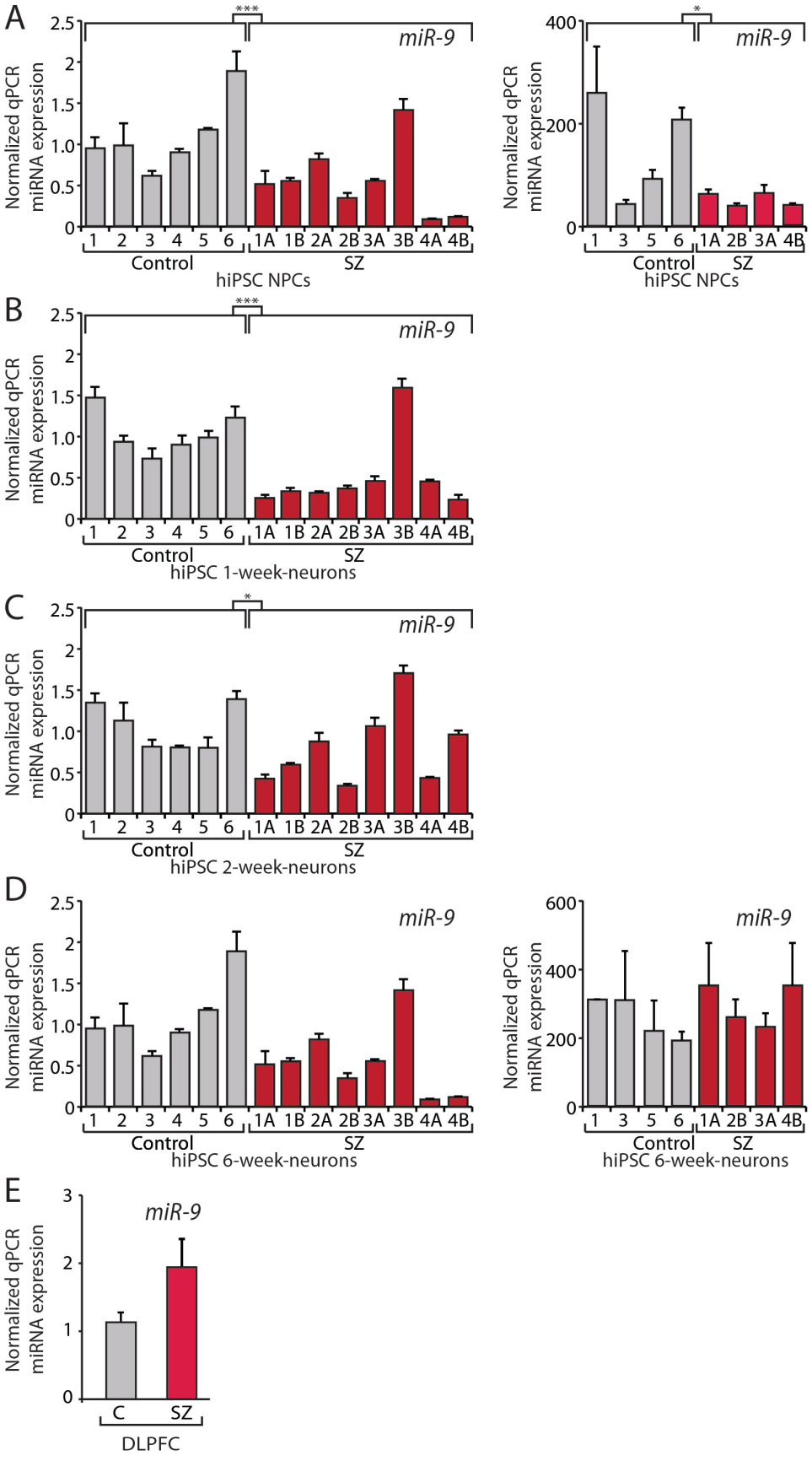
A
B
C
D
E
miR-9
Normalized qPCR miRNA expression
***
*
1 2 3 4 5 6 1A 1B 2A 2B 3A 3B 4A 4B
1 3 5 6 1A 2B 3A 4B
Control
SZ
hiPSC NPCs
hiPSC 1-week-neurons
hiPSC 2-week-neurons
hiPSC 6-week-neurons
C
DLPFC

**SI Fig. 1. Decreased miR-9 levels occur in SZ NPCs but not SZ hiPSC forebrain neurons, presented by individual, related to Figure 1.**

**A-D.** Experimental replicates, by NPC line and experimental replication, of the qPCR validation of normalized miR-9 expression during the differentiation of SZ NPCs (**A**) into 1- (**B**), 2- (**C**) and 6-week-old (**D**) neurons. **E.** qPCR of normalized miR-9 expression in post-mortem DLPFC tissue from ten SZ patients and ten controls. Error bars are s.e., *P < 0.05, **P < 0.01, ***P < 0.001.

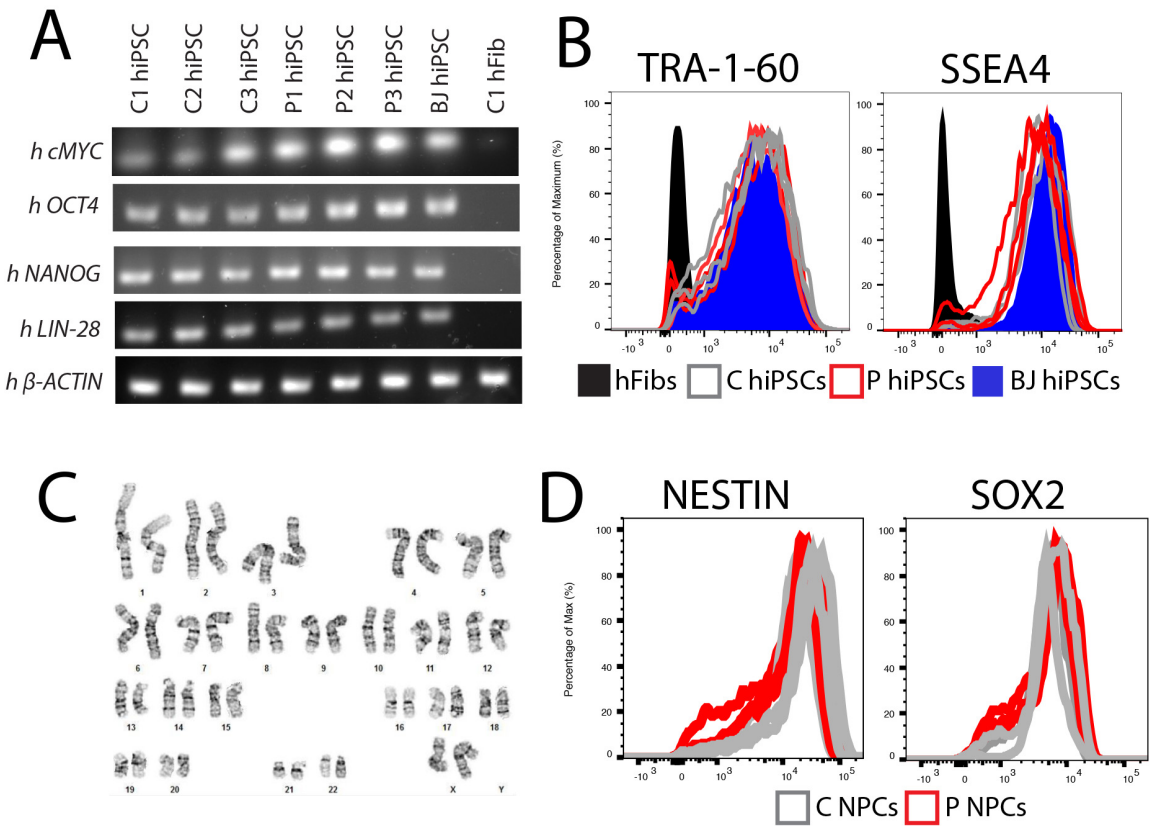


**SI Fig. 2. Validation of COS hiPSCs and NPCs, related to Figure 1.**

**A.** RT-PCR gels showing that hiPSCs derived from both control (C) and childhood-onset-SZ (COS) patient (P) fibroblasts expressed the human pluripotency markers *cMYC*, *OCT4*, *NANOG* and *LIN-28*. RT-PCR results from validated BJ (ATCC CRL-2522) hiPSCs and a control fibroblast cell line are also displayed as positive and negative controls, respectively. **B.** Flow cytometry histograms for TRA-1-60 (left panel) and SSEA4 (right panel), black filled trace (control fibroblast cell line), grey trace (control hiPSCs), red trace (COS patient hiPSCs) and blue filled trace (BJ hiPSCs). **C**. A representative karyotype image from a COS patient derived hiPSC line showing no chromosomal abnormalities. **D**. Flow cytometry histograms demonstrating that control (grey) and COS patient (red) hiPSC-derived NPCs express NESTIN (left panel) and SOX2 (right panel).

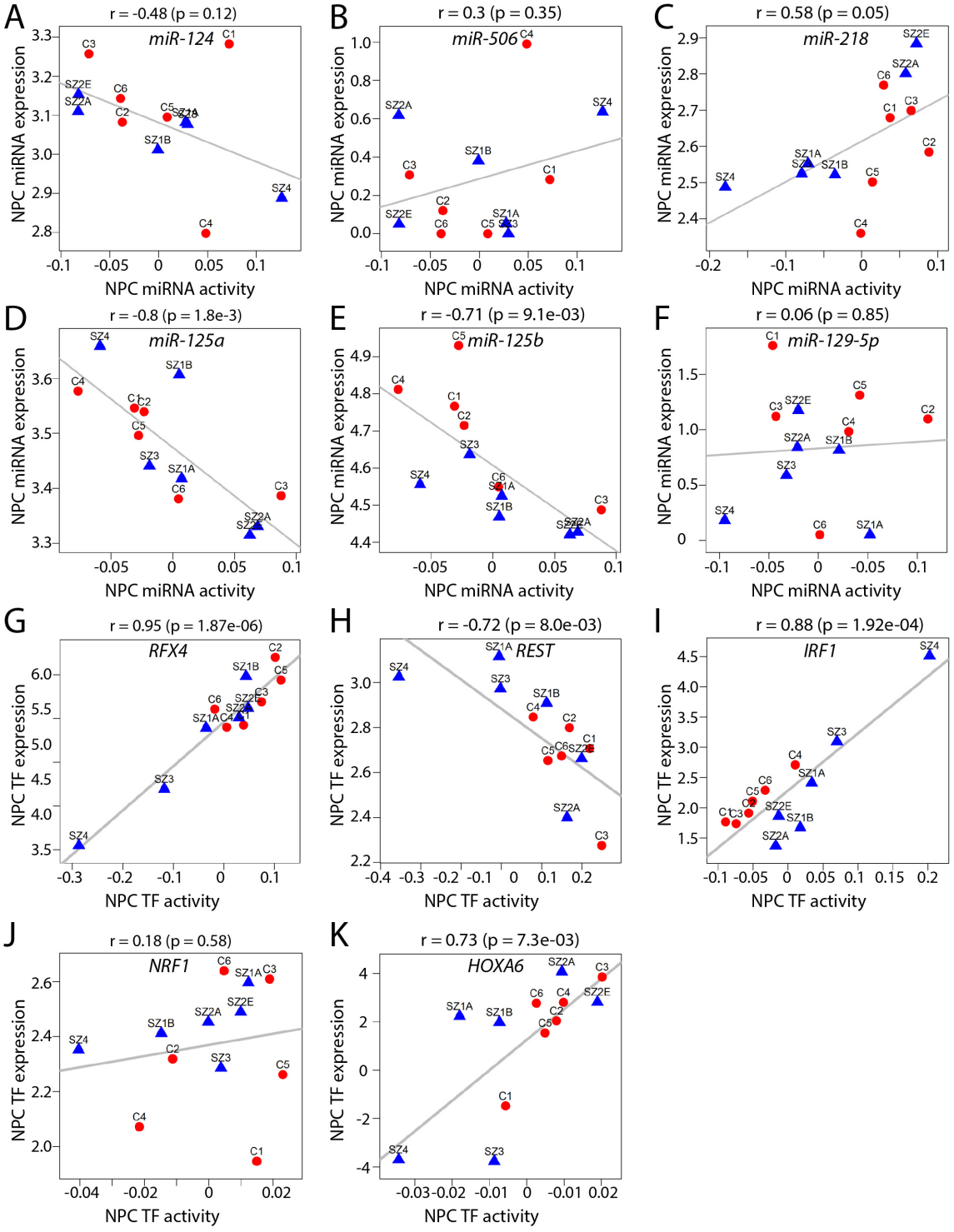


**SI Fig. 3. Additional top miRNAs and transcription factors with change of activities predicted by the integrative model, related to Figure 2.**

**A-F.** Additional top miRNAs. Scatter plots between expression and predicted change of activities for miRNA-124 (**A**), miR-506 (**B**), miR-218 (**C**), miR-125a (**D**), miR-125b (**E**) and miR-129 (**F**). **G-K.** Top transcription factors. Scatter plots between expression and predicted change of activities for RFX4 (**G**), REST (**H**), IRF1 (**I**), NRF1 (**J**) and HOXA6 (**K**).

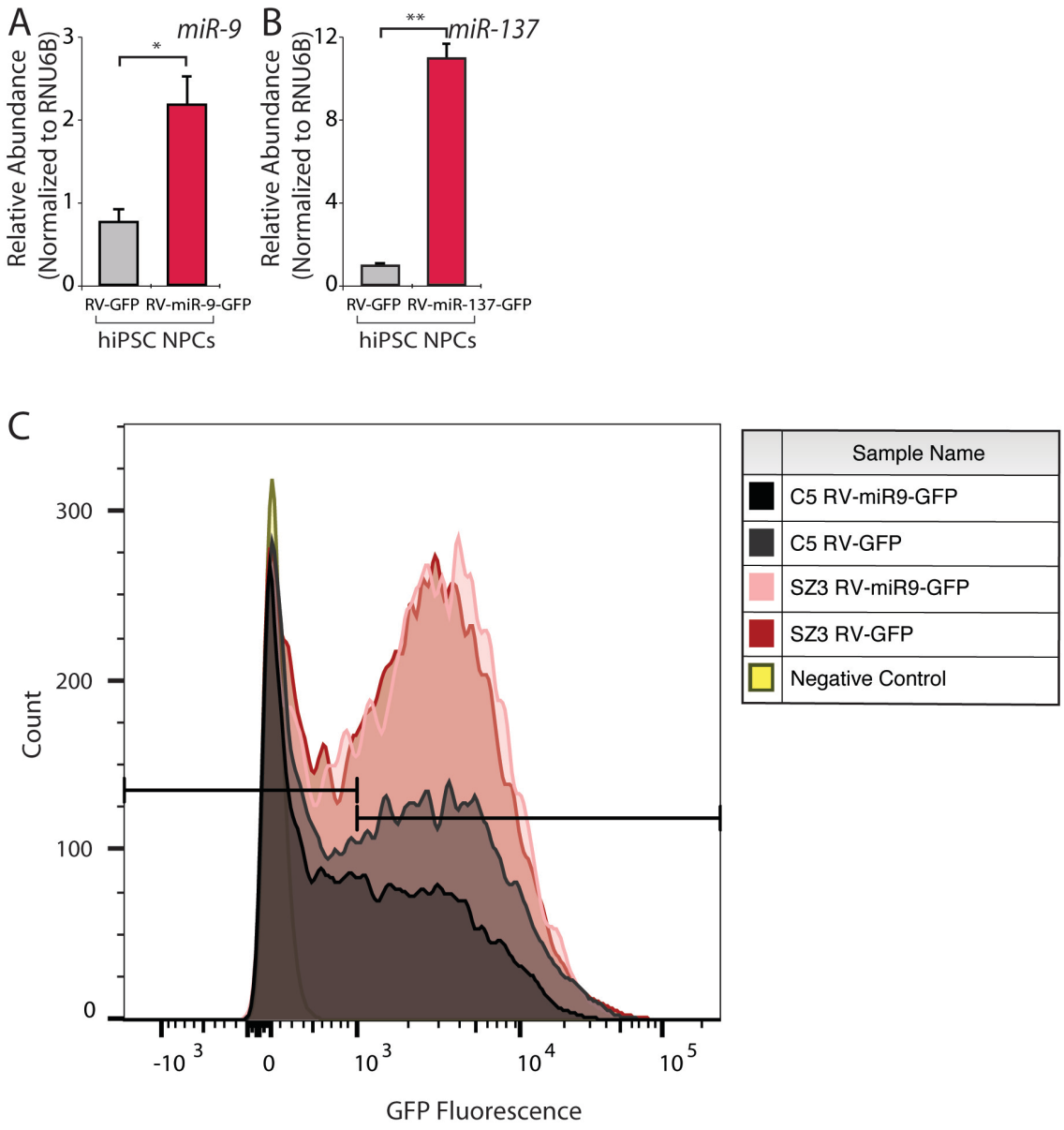


**SI Fig. 4. Validation of RV overexpression constructs, related to Figure 3.**

**A-B.** qPCR validation that RV-miR-9 (**A**) and RV-miR-137 (**B**) overexpression in hiPSC forebrain NPCs result in increased miR-9 and miR-137 levels, respectively. **C**. FACS purification of GFP-positive cells from RV-GFP and RV-miR-9 transduced control and SZ NPCs prior to RNAseq analysis. Error bars are s.e., *P < 0.05, **P < 0.01, ***P < 0.001.

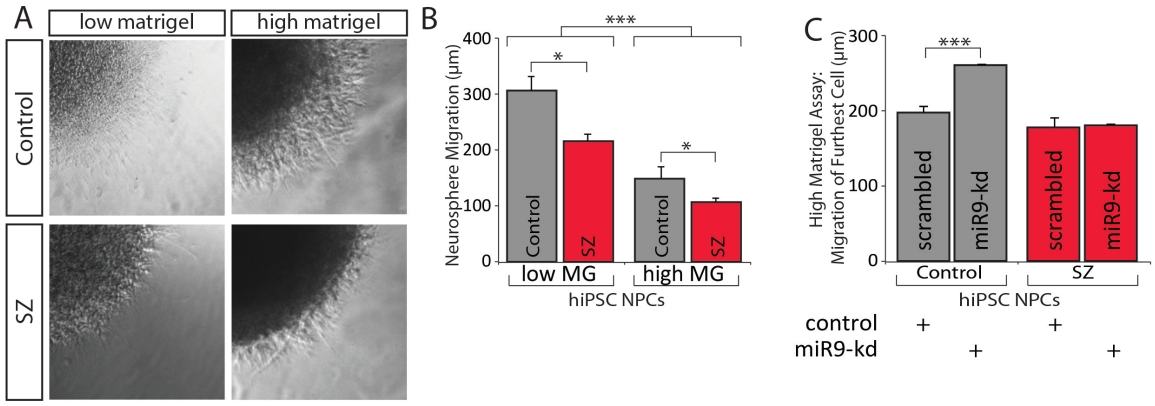


**SI Fig. 5. Aberrant migration in SZ hiPSC forebrain NPCs, related to Figure 3.**

**A.** Brightfield images of neurosphere outgrowth in high (Delaloy et al., 2010) and low (Brennand et al., 2014) matrigel conditions, revealing different neurospheres morphologies between the two conditions. **B.** Neurosphere outgrowth by untranduced control and SZ hiPSC forebrain NPCs, in either high or low matrigel conditions. **C.** Neurosphere migration in high matrigel conditions by control and SZ hiPSC NPCs, following transient reduction of miR-9 levels. Migration distance was calculated as the average of the five furthest migrating cells, as in Delaloy *et al*. (2010). Error bars are s.e., *P < 0.05, **P < 0.01, ***P < 0.001.

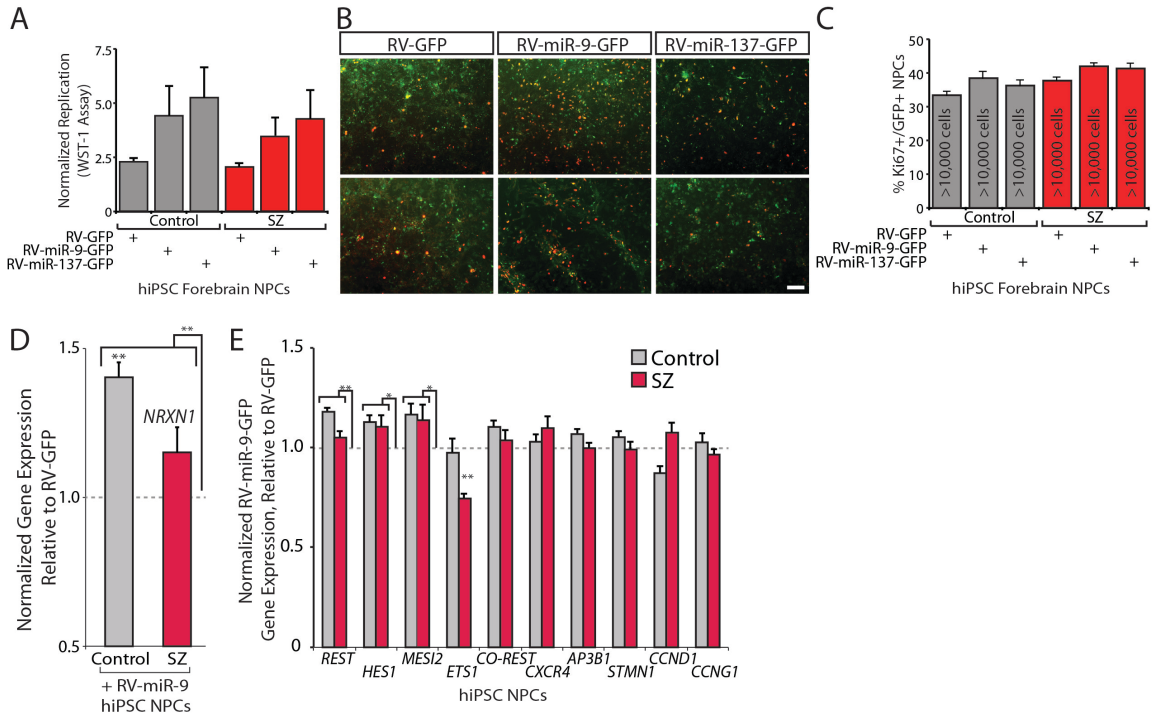


**SI Fig. 6. Effect of manipulation miR-9 on replication and target gene expression, related to Figures 3 and 4.**

**A.** WST-1 cell viability assay. 24-hour cell viability in control and SZ hiPSC forebrain NPCs, relative to time 0 hour, following stable transduction with RV-GFP, RV-miR-9 or RV-miR137, when assayed by comparing absorbance of WST-1 converted to formazan dye by cellular reductases. **B.** Control and SZ hiPSC forebrain NPCs transduced with RV-GFP, RV-miR-9 or RV-miR137 and stained with the cell cycle marker Ki67 (red). DAPI-stained nuclei (blue). Scale bar 100 μm. **C.** Cell counts for the percentage of GFP-positive control or SZ hiPSC forebrain NPCs, stably transduced with either RV-GFP, RV-miR-9 or RV-miR137, that are positive for the cell cycle protein Ki67 of control and SZ hiPSC forebrain NPCs. **D.** Nanostring nCounter analysis of fold-change of normalized expression of the neural adhesion gene *NRXN1* following stable overexpression of RV-miR-9-GFP, relative to expression in RV-GFP transduced (gray dashed line) control and SZ NPCs. **E.** Nanostring nCounter analysis of fold-change of normalized expression of selected known miR-9 target genes, following stable overexpression of RV-miR-9-GFP, relative to expression in RV-GFP transduced (gray dashed line) control and SZ NPCs. Error bars are s.e. *P < 0.05, **P < 0.01, ***P < 0.001.

A

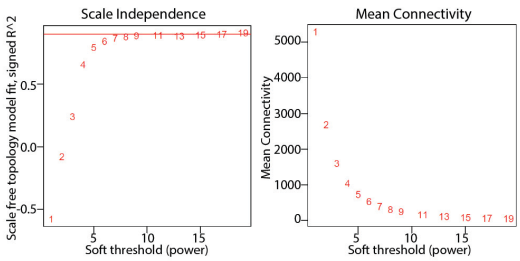


B

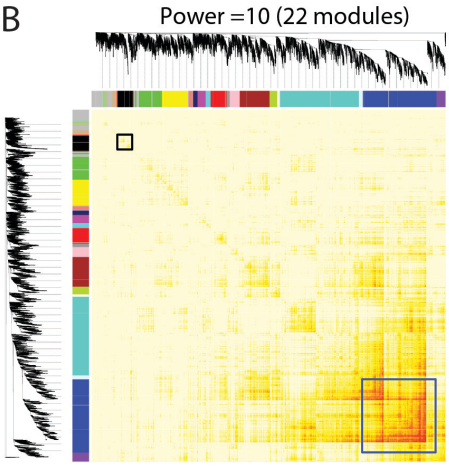


**Cell Migration**
**(Black: 585 genes) Eigengene differential expression p=0.25**
extracellular region (p=3.83e-13)
extracellular matrix (p=9.39e-12)
extracellular matrix organization (p=9.65e-12)
extracellular structure organization (p=9.65e-12)
proteinaceous extracellular matrix (p=4.25e-10)
cell adhesion (p=4.67e-10)
extracellular space (p=7.60e-10)
peptide cross-linking (p=3.65e-09)
extracellular matrix structural constituent (p=1.61e-08)
Collagen (p=2.74e-08)

**Neural Development**
**(Blue: 2876 genes) Eigengene differential expression p=9.6e-03**
intrinsic to membrane (p=3.66e-08)
integral to membrane (p=1.09e-07)
membrane part (p=4.86e-07)
Membrane (p=5.38e-07)
plasma membrane part (p=4.56e-06)

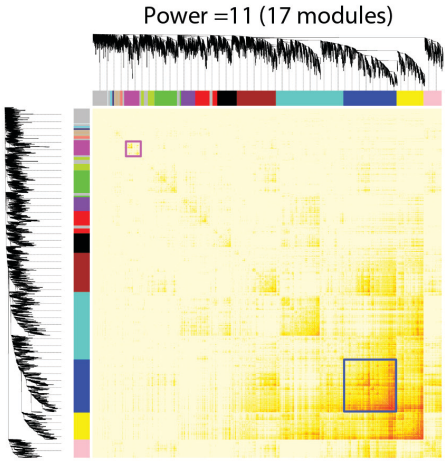


**Cell Adhesion**
**(Magenta: 601 genes) Eigengene differential expression p=0.25**
extracellular matrix(p=3.19e-10)
extracellular region(p=2.10e-09)
proteinaceous extracellular matrix(p=3.24e-09)
extracellular space(p=3.78e-07)
extracellular matrix organization(p=8.48e-07)
extracellular structure organization(p=8.48e-07)
cell adhesion(p=1.31e-06)

**Cell Migration**
**(Blue: 2103 genes) Eigengene differential expression p=5.37e-04**
negative regulation of protein complex disassembly(p=7.56e-07)
regulation of protein depolymerization(p=8.61e-07)
negative regulation of actin filament depolymerization(p=9.77e-07)
regulation of protein complex disassembly(p=2.05e-05)
negative regulation of cytoskeleton organization(p=2.95e-05)
homophilic cell adhesion(p=4.44e-05)
actin filament depolymerization(p=5.88e-05)
compartment pattern specification(p=9.20e-05)
negative regulation of actin filament polymerization(p=1.80e-04)
actin filament capping(p=1.98e-04)

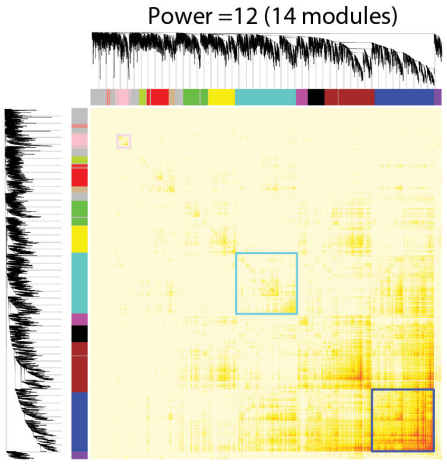


**Cell Adhesion**
**(Pink: 543 genes) Eigengene differential expression p=0.4**3
extracellular matrix(p=4.18e-12)
extracellular region p=5.64e-12)
proteinaceous extracellular matrix p=6.11e-11)
extracellular matrix organization p=1.10e-10)
extracellular structure organization p=1.10e-10)
cell adhesion p=1.09e-09)
extracellular space p=8.75e-09)

**Cell migration**
**(Turquoise: 2420 genes) Eigengene differential expression p=1.70e-03**
positive regulation of cellular component movement(p=2.04e-04)
positive regulation of cell motility(p=3.141e-04)
positive regulation of cell migration(p=3.35e-04)
cell migration(p=0.000371332e-04)
wound healing(p=587074e-04)
positive regulation of locomotion(p=7.53e-04)

**Neural Migration**
**(Blue: 2343 genes) Eigengene differential expression p=5.41e-04**
negative regulation of protein complex disassembly (p=4.27e-06)
negative regulation of cytoskeleton organization (p=1.99e-05)
regulation of protein depolymerization (p=2.26e-05)
negative regulation of actin filament depolymerization (p=2.66e-05)
intrinsic to membrane (p=2.83e-05)
nervous system development (p=3.24e-05)
plasma membrane part (p=3.54e-05)
integral to membrane (p=3.94e-05)
developmental process (p=4.48e-05)
multicellular organismal development (p=5.77e-05)

**SI Fig. 7. Effect of manipulating miR-9 levels on global gene expression, related to Figure 4.**

**A**. Selection of soft-thresholding powers for WGCNA. The left panel shows the scale-free fit index (y-axis) as a function of the power parameter (x-axis). The right panel displays the mean connectivity (degree, y-axis) as a function of the power parameter (x-axis). **B**. The coexpression network visualization using heatmap, with module assignment and gene dendrogram shown along the left side and the top. Larger gene interaction magnitude is marked by darker colors. Blocks along the diagonal are the modules. As shown in (**A**), the power of 11 shows the best scale-free topology fit. The networks with different powers (10 to 12) were also shown. Consistently, migration-related modules are enriched in all the four networks.

## SI EXPERIMENTAL PROCEDURES

*Description of SZ patients, hiPSC reprogramming and NPC differentiation*

| Cohort | ID in Figures | Patient ID | hiPSC Lines ID | NPC Line ID | Family | Sex | Dx | Ethnicity | Age of Onset | IQ | Developmental History | Clozapine Response | Family History | SZ-related CNV Burden | rs181900 Genotype |
|---|---|---|---|---|---|---|---|---|---|---|---|---|---|---|---|
| 1 | C1 | BJ | BJ-2 | BJ-2-A | n/a | M | Control | Causasian | - | unknown | unknown | unknown | unknown | - | CC |
| 1 | C2 | GM034 | 3440-5 | 3440-5-A | n/a | M | Control | Causasian | - | unknown | unknown | unknown | unknown | - | CC |
| 1 | C3 | GM036 | 3651-A | 3651-A-A | n/a | F | Control | Causasian | - | unknown | unknown | unknown | unknown | - | CC |
| 1 | C4 | GM045 | 4506-B | 4506-B-A | n/a | F | Control | Causasian | - | unknown | unknown | unknown | unknown | - | CC |
| 1 | C5 | AG0931 | 9319-2 | 9319-2-A | n/a | F | Control | Causasian | - | unknown | unknown | unknown | unknown | - | CC |
| 1 | C6 | AG0942 | 9429-3 | 9429-3-A | n/a | F | Control | Causasian | - | unknown | unknown | unknown | unknown | - | CC |
| 1 | SZ1 | GM020 | 2038-1 | 2038-1-A, 2038-1-B | Proband | M | Schizophrenia | Causasian | 6 | unknown | unknown | unknown | unknown | - | CC |
| 1 | SZ2 | GM017 | 1792-1 | 1792-1-A, 1792-1-E | Proband 1 | M | Schizophrenia | Causasian Jewish /Scandanavian | unknown | unknown | unknown | unknown | SZ, SA, ASD | - | CC |
| 1 | SZ3 | GM018 | 1835-1 | 1835-1-3, 1835-1-5 | Sibling 1 | F | Schizo-affective | Causasian Jewish | unknown | unknown | unknown | unknown | SZ, ASD | - | CC |
| 1 | SZ4 | GM024 | 2497-1 | 2497-1-B, 2497-1-C | Proband | M | Schizophrenia | Causasian Jewish | 15 | unknown | unknown | unknown | SZ, SPD | - | AC |
| 2 | C1 | 2607 | 2607-1, 2607-4 | 2607-1-A,2607-4-1 | n/a | M | Control | Caucasian | n/a | 126 | clean | n/a | - | - | CC |
| 2 | C2 | 3113 | 3113-1, 3113-2 | 3113-1-4, 3113-2-1 | n/a | F | Control | Caucasian | n/a | 123 | clean | n/a | - | - | CC |
| 2 | C3 | 3121 | 3121-1, 3121-2 | 3121-1-4, 3121-2-1 | n/a | F | Control | Caucasian | n/a | 134 | clean | n/a | - | - | CC |
| 2 | C4 | 3130 | 3130-2, 3130-4 | 3130-2-1, 3130-4-21 | n/a | M | Control | Caucasian | n/a | 114 | clean | n/a | - | - | CC |
| 2 | C5 | 3182 | 3182-2 | 3182-2-4 | n/a | F | Control | Caucasian | n/a | 119 | clean | n/a | - | - | CC |
| 2 | C6 | 3183 | 3183-3 | 3183-3-4, 3183-3-1 | n/a | F | Control | Caucasian | n/a | 117 | clean | n/a | - | - | CC |
| 2 | C7 | 3188 | 3188-2A | 3188-2A-4 | n/a | F | Control | Caucasian | n/a | 107 | clean | n/a | - | - | CC |
| 2 | C8 | 3234 | 3234-1, 3234-2, 3234-3 | 3234-1-4, 3234-2-4, 3234- | n/a | M | Control | Indian | n/a | 94 | clean | n/a | - | - | CC |
| 2 | C9 | 553 | 553-2, 553-3 | 553-2-3, 553-3-1 | n/a | M | Control | Caucasian | n/a | 127 | clean | n/a | - | - | CC |
| 2 | C10 | 690 | 690-1, 690-4 | 690-1-4, 690-2-4, 690-3-4 | n/a | M | Control | Caucasian | n/a | 115 | clean | n/a | - | - | CC |
| 2 | COS1 | 1275 | 1275-B,1275-C | 1275-B-3,1275-C-1 | Proband | F | COS | Caucasian | 10 | 67 | MDD | NA | SPD | 22q11.2 | CC |
| 2 | COS2 | 1442 | 1442-4, 1442-3 | 1442-4-3, 1442-3-2 | Proband | M | COS | Caucasian | 12 | 74 | ASD | N | ASD | 1p33 | CC |
| 2 | COS3 | 2011 | 2011-3, 2011-4 | 2011-3-2, 2011-4-2 | Proband | F | COS | Caucasian | 8 | 69 | MDD | Y | SPD; PPD | 16p11.2 | CC |
| 2 | COS4 | 2476 | 2476-1 | 2476-1-4, 2476-1-4r2 | Proband | F | COS | Caucasian-Hispanic | 8 | 82 | clean | Y | APD | - | CC |
| 2 | COS5 | 2513 | 2513-2, 2513-1 | 2513-2-1, 2513-1-1 | Proband | M | COS | Caucasian | 4 | 55 | ASD | N | BD | - | CC |
| 2 | COS6 | 2620 | 2620-B, 2620-C | 2620-B-4 2620-C-3 | Proband | M | COS | Caucasian | 11 | 54 | clean | N | APD, SPD | - | CC |
| 2 | COS7 | 2962 | 2962-1, 2962-3 | 2962-1-4, 2962-3-21 | Proband | M | COS | Caucasian-Hispanic | 8 | 78 | clean | Y | SZ/ASD | - | CC |
| 2 | COS8 | 499 | 449-5, 449-2 | 449-5-2, 449-2-12 | Proband | M | COS | Caucasian | 12 | 84 | clean | N | SPD | 3p25.3 | CC |
| 2 | COS9 | 581 | 581-1 | 581-1-2, 581-1-2n2 | Proband | M | COS | Caucasian | 7 | 74 | MDD | N | SA | 2p16.3 del | CC |
| 2 | COS10 | 676 | 676-1, 676-2 | 676-1-2, 676-2-3 | Proband | F | COS | Caucasian | 10 | 79 | MDD | N | PPD | 16p11.2 | CC |

For cohort #1, patient and control NPCs were differentiated from hiPSCs reprogrammed from fibroblasts obtained from Coriell or ATCC. NPCs from four patients and six controls were compared (Brennand et al., 2015; Brennand et al., 2011). Cohort 1 NPC lines used in each assay is summarized below:

| DIAGNOSIS | Control | Control | Control | Control | Control | Control | SZ | SZ | SZ | SZ |
|---|---|---|---|---|---|---|---|---|---|---|
| Sample ID | BJ | GM03440 | GM03651 | GM04506 | AG09319 | AG09429 | GM02038 | GM01792 | GM01835 | GM02497 |
| Patient ID | C1 | C2 | C3 | C4 | C5 | C6 | P1 | P2 | P3 | P4 |
| Validated hiPSC lines | 4 | 1 | 1 | 1 | 1 | 1 | 2 | 2 | 2 | 2 |
| NPC lines for microarray | 1 | 0 | 1 | 0 | 1 | 1 | 1 | 1 | 1 | 1 |
| NPC lines for qPCR | 3 | 1 | 1 | 1 | 1 | 1 | 2 | 2 | 2 | 2 |
| Nanostring miRNA NPC | 1 | 1 | 1 | 1 | 1 | 1 | 2 | 2 | 1 | 1 |
| NPC passage | 9 | 9 | 7 | 9 | 10 | 8 | 8, 7 | 7, 7 | 7, 7 | 6, 8 |
| Nanostring miRNA Neuron | 1 | 1 | 1 | 1 | 1 | 1 | 2 | 2 | 2 | 0 |
| NPC passage | 9 | 9 | 7 | 9 | 10 | 8 | 8, 7 | 7, 7 | 7, 7 | 6, 8 |
| RNASeq SZ NPC signature | 1 | 1 | 1 | 1 | 1 | 1 | 2 | 2 | 1 | 1 |
| NPC passage | 9 | 9 | 7 | 9 | 10 | 8 | 8, 7 | 7, 7 | 7 | 6, 8 |
| RNASeq SZ neuron signature | 1 | 1 | 1 | 1 | 1 | 1 | 2 | 1 | 2 | 0 |
| NPC passage | 9 | 9 | 7 | 9 | 10 | 8 | 8, 7 | 7 | 7,7 | - |
| RNAseq miR-9 perturbation | 0 | 1 | 0 | 0 | 1 | 0 | 1 | 0 | 1 | 0 |
| NPC passage | - | 8 | - | - | 9 | - | 7 | - | 7 | - |
| Nanostring miR target NPC | 1 | 1 | 1 | 1 | 1 | 1 | 2 | 2 | 1 | 1 |
| LC MS/MS NPC | 1 | 1 | 1 | 1 | 1 | 1 | 2 | 2 | 2 | 2 |
| NPC lines for RV neurosphere assay | 3 | 1 | 1 | 2 | 1 | 1 | 2 | 2 | 2 | 2 |
| replicate #1 2013 01 07 | 2 | 1 | 1 | 2 | 1 | 1 | 2 | 3 | 1 | 2 |
| replicate #2 2013 03 06 | 2 | 1 | 0 | 1 | 1 | 1 | 2 | 2 | 1 | 2 |
| replicate #3 2013 11 Chelsea | 1 | 1 | 1 | 1 | 1 | 1 | 2 | 2 | 2 | 2 |
| replicate #4 2013 8 7 Chelsea | 3 | 1 | 1 | 1 | 1 | 1 | 2 | 2 | 2 | 2 |
| replicate #5 2014 01 07 Ngoc | 1 | 1 | 1 | 1 | 1 | 1 | 2 | 2 | 2 | 0 |
| replicate #6 2014 03 Ngoc | 1 | 1 | 1 | 1 | 1 | 1 | 2 | 2 | 2 | 0 |
| NPC lines for high concentration neurosphere assay | 2 | 1 | 1 | 1 | 1 | 1 | 2 | 2 | 2 | 2 |
| replicate #1 2013 06 06 | 2 | 1 | 1 | 1 | 1 | 1 | 2 | 2 | 2 | 2 |
| replicate #1 2013 06 13 | 2 | 1 | 1 | 1 | 1 | 1 | 1 | 2 | 2 | 2 |
| NPC lines for miR9 knockdown | 3 | 1 | 1 | 1 | 1 | 1 | 2 | 2 | 2 | 2 |
| replicate #1 | 1 | 1 | 0 | 0 | 0 | 0 | 0 | 0 | 0 | 0 |
| replicate #2 | 1 | 1 | 1 | 0 | 1 | 1 | 0 | 0 | 0 | 0 |
| NPC lines for miR9 knockdown in high MG | 3 | 1 | 1 | 1 | 1 | 1 | 2 | 2 | 2 | 2 |
| replicate #1 2013 06 28 | 3 | 1 | 1 | 1 | 1 | 1 | 2 | 2 | 2 | 2 |
| replicate #2 2014 2 27 | 1 | 1 | 1 | 1 | 1 | 0 | 2 | 1 | 2 | 0 |

For cohort #2, fibroblast biopsies were obtained from patients with childhood-onset-SZ (COS) and unrelated controls that were recruited as part of a longitudinal study Dr. Judith Rapoport (NIMH) (Eckstrand et al., 2008; Gogtay et al., 2004; McCarthy et al., 2009; Shaw et al., 2006; Sporn et al., 2004).

All participants provided assent/consent with written informed consent from a parent or legal guardian for minors. Fibroblasts were derived at NIMH and de-identified samples were transferred to the Icahn School of Medicine at Mount Sinai (ISMMS). This study was approved by the Institutional Review Boards of the NIMH and the ISMMS. HFs were cultured on plates coated with 0.1% gelatin (in milli-Q water) and grown in HF media. hiPSCs were derived as described previously (Lee et al., 2015); replicating but nearly confluent HFs were transfected with Cytotune Sendai virus (ThermoFisher Scientific). Cells were allowed to recover for at least 3 days, dissociated with TrypleE (ThermoFisher Scientific) and re-plated onto a 10-cm dish containing 1 million mouse embryonic fibroblasts (mEFs). Cells were switched to HUES media (DMEM/F12 (Invitrogen), 20% KO-Serum Replacement (Invitrogen), 1x Glutamax (Invitrogen), 1x NEAA (Invitrogen), 1x 2 - mercaptoethanol (Sigma) and 20 ng/ml FGF2 (R&D Systems)) and fed every 2-3 days. hiPSC colonies were manually picked and clonally plated onto 24-well mEF plates in HUES media. At early passages, hiPSCs were split through manual passaging, but at higher passages, hiPSC could be enzymatically passaged with Collagenase (1mg/ml in DMEM) (Sigma). Karyotyping analysis was performed by Wicell Cytogenetics (Madison WI); only karyotypically normal lines were used for subsequent studies.

Cohort 2 COS NPCs were generated in a similar method to Cohort 1 (Brennand et al., 2015; Brennand et al., 2011), although differentiated with dual-SMAD inhibition (Chambers et al., 2009) to improve yield, as described (Topol et al., 2015); five controls from Cohort 2 were published previously (Lee et al., 2015). Incubation with Collagenase (1 mg/ml in DMEM) at 37°C for 1-2 hours lifted colonies, which were transferred to a nonadherent plate (Corning). Embryoid Bodies (EBs) were grown in suspension with dual-SMAD inhibition (0.1mM LDN193189 (Stemgent) and 10mM SB431542 (Tocris)) N2/B27 media (DMEM/F12-Glutamax (Invitrogen), 1x N2 (Invitrogen), 1X B27 (Invitrogen)). 7-day-old EBs were plated in N2/B27 media with 1 μg/ml Laminin (Invitrogen) onto poly-ornithine /Laminin-coated plates. Neural rosettes were harvested from 14-day-old EBs using STEMdiff™ Neural Rosette Selection Reagent (Stem Cell Technologies) for 60 minutes at 37°C before being plated in NPC media (DMEM/F12, 1x N2, 1x B27-RA (Invitrogen), 1 μg/ml Laminin and 20 ng/ml FGF2 on poly-ornithine/laminin-coated plates.

Using a PsychChip SNP array we evaluated shared genetic background for all cell lines used in this study, which confirmed that GM01792 and GM01835 are siblings, but found no substantial relatedness between the other individuals in Cohorts 1 or 2.

*NPC culture*

As previously reported, spatial patterning, replication and propensity towards neuronal differentiation of NPCs does not appear to vary based on psychiatric diagnosis (Brennand et al., 2015; Brennand et al., 2011).

NPCs were maintained at high density, grown on Matrigel in NPC media (DMEM/F12, 1x N2, 1x B27-RA (Invitrogen), 1 μg/ml Laminin (Invitrogen) and 20 ng/ml FGF2 (Invitrogen) and split approximately 1:3-1:4 every week with Accutase (Millipore) (Brennand et al., 2011). NPCs can be expanded beyond 10 passages.

NPC experiments were conducted on passage-matched populations, typically between passages five and ten. Beyond this, NPCs can show an increased propensity for astrocyte differentiation, or undergo spontaneous transformation. At any point, if an NPC line showed evidence of either decreased neuronal differentiation or cellular transformation, it was eliminated from analysis.

*Gene and miRNA expression analysis*

For Nanostring gene expression studies, Nanostring Technologies designed probe sets. For Nanostring gene expression studies, Nanostring Technologies designed probe sets. Neural targets of miR-9 include REST and CO-REST (Packer et al., 2008; Yoo et al., 2009), TLX (NR2E1) (Zhao et al., 2009), HES1 (Bonev et al., 2012), CXCR4 (Yu et al., 2014), FOXG1 (Shibata et al., 2008), STMN1 (Delaloy et al., 2010), FOXO1 (Senyuk et al., 2013), AP3B1 (Selcuklu et al., 2012), CCNG1 (Selcuklu et al., 2012), CCND1 (Zheng et al., 2013), ETS1 (Zheng et al., 2013) and MEIS2 (Shibata et al., 2011). Nanostring gene expression analysis was performed on purified RNA as recommended. For mRNA, analysis was performed using nCounter2.0 software, with background correction; mRNA levels were normalized to β-ACTIN and GAPDH levels and samples flagged by nCounter2.0 as having normalization errors were discarded from analysis.

For miRNA qPCR, quantification of the mature form of miRNAs was performed using the TaqMan miRNA assays (ThermoFisher Scientific). Endogenous U6 small nuclear RNA (snRNA) and RNU48 were used as controls.

For qPCR, cDNA was synthesized using Superscript III at 50°C for one to two hours, inactivated for 15 minutes at 70°C and then treated with RNAaseH for 15 minutes at 37°C, inactivated with EDTA and heated to 70°C for 15 minutes. qPCR was performed using SybrGreen.

*Integration of RNAseq datasets and all new analyses*

For the "miR-9 perturbation" RNAseq data, paired t-test was used to compare samples transiently transfected with scrambled or miR-9 LNA probes, and compare samples transduced with RV-GFP or RV-miR-9-GFP with. To check the consistency of DE between "miR-9 perturbation" dataset (low miR-9 vs. high miR-9 samples) and Coriell dataset (SZ versus Control), we carried out the enrichment analysis with Fisher's exact test. Furthermore, motivated by our observation that the effect of miR-9 overexpression is more apparent in SZ (compared to control) and the effect of miR-9 knockdown is more apparent in control (compared to SZ), we performed the DE enrichment analysis of Coriell dataset for two subsets of "miR-9 perturbation" dataset: one is composed of SZ versus SZ-miR-9-overexpression and Control-miR-9-knockdown versus Control, and the other is composed of SZ-miR-9-knockdown versus SZ and Control versus Control-miR-9-overexpression.

To assess the effect of "miR-9 perturbation" on its target genes, we first obtained gene expression fold changes for predicted miR-9 targets (TargetScan 6.0) (Creighton et al., 2008) from each pairwise comparison (each perturbation and its control as described above), and used the first principal component from a principal component analysis as the representative miR-9 target gene expression fold change to correlate with the miR-9 fold change obtained from qPCR. We also applied the global integrative model to the "miR-9 perturbation" dataset, with non-redundant miR-9 activity obtained for each sample as done for the Coriell cohort (SZ vs. control hiPSCs). In addition, the weighted gene co-expression network analysis (WGCNA) was applied to the "miR-9 perturbation" dataset under the parameter setting selected using scale-free criterion (Zhang and Horvath, 2005). GO enrichment analysis was carried out for each coexpression module using the R function within WGCNA package. Similar to calling gene differential expression for "miR-9 perturbation" data, the paired t-test was applied to the eigengene of each module to assess the module differential expression (Zhang and Horvath, 2005).

Results from the PGC GWAS (Schizophrenia Working Group of the Psychiatric Genomics Consortium, 2014) were intersected with the "miR-9 perturbation" DE using a competitive gene-set enrichment analysis as implemented into MAGMA (de Leeuw et al., 2015). In a first step HUGO IDs were translated into ENTREZ IDs for all genes in the analysis. Subsequently SNPs were annotated to these genes (no flanking sequence allowed) using MAGMA and the NCBI36.3 genome build. Gene-based p-values were calculated using the PGC summary stats after filtering for MAF (0.01) and INFO scores (0.8) and only taking SNPs into account that could be directly mapped to autosomal genes. Data from the 1000 genomes reference population (Europeans only; (Genomes Project et al., 2012)) were used to estimate correlation structure for all markers in the analysis. We tested three different gene-sets for enrichment in genes associated with SZ: a) all genes in the "miR-9 perturbation" DE list, b) all predicted targets of miR-9 (TargetScan v6.0), and c) all genes in the "miR-9 perturbation" DE list that are not in the TargetScan list of predicted targets of miR-9. Reported p-values are not corrected for multiple testing.

*Neurosphere migration assay*

NPCs were dissociated with accutase and then cultured for 48 hours in nonadherent plates to generate neurospheres. Neurospheres were manually picked and cultured in "low" (0.05 mg/ml) Matrigel matrix (0.5 mg Matrigel was plated in cold NPC media on a 96-well plate 1 hour prior to neurosphere plating; following neurosphere picking, an additional 0.5 mg Matrigel was added in cold NPC media per 96-well plate). DAPI-stained neurospheres were imaged at 48 hours. Average radial migration from each neurosphere was measured using NIH ImageJ. A quantification of the total number of neurospheres analyzed in each assay can be found below:

| DIAGNOSIS | Control | Control | Control | SZ | SZ | SZ |
|---|---|---|---|---|---|---|
| **RV-overexpression** | **GFP** | **miR-9** | **miR-137** | **GFP** | **miR-9** | **miR-137** |
| Total neurospheres analyzed | 375 | 287 | 133 | 416 | 328 | 151 |
| replicate #1 2013 01 07 | 92 | 85 | 0 | 79 | 86 | 0 |
| replicate #2 2013 03 06 | 81 | 75 | 0 | 80 | 76 | 0 |
| replicate #3 2013 11 | 70 | 69 | 0 | 106 | 107 | 0 |
| replicate #4 2013 8 7 | 78 | 0 | 79 | 95 | 0 | 89 |
| replicate #5 2014 03 | 54 | 58 | 54 | 56 | 59 | 62 |
| **miRNA knockdown** | **scrambled** | **miR-9** | **miR-137** | **scrambled** | **miR-9** | **miR-137** |
| Total neurospheres analyzed | 166 | 154 | 0 | 126 | 130 | 0 |
| replicate #1 2013 06 28 | 44 | 45 | not tested | 45 | 48 | not tested |
| replicate #2 2015 09 | 22 | 25 | not tested | not tested | not tested | not tested |
| replicate #3 2015 10 | 54 | 36 | not tested | 41 | 43 | not tested |
| replicate #4 2014 2 27 high MG | 46 | 48 | not tested | 40 | 39 | not tested |
| **Control vs SZ (High matrigel)** | | | | | | |
| replicate #1 2013 06 06 | 8 | not tested | not tested | 15 | not tested | not tested |
| replicate #2 2013 06 13 | 9 | not tested | not tested | 12 | not tested | not tested |

We note that our findings are inconsistent with increased migration in control human embryonic stem cell (hESC)-derived NPCs reported following knockdown of miR-9 (Delaloy et al., 2010). To resolve this contradiction, we investigated further; Delaloy *et al* employed 264-fold higher concentrations of Matrigel (13.2 mg/ml) than used in our assays in order to create a "3D" migration condition, one that results in markedly different neurosphere morphology (**SI Fig. 5A**). In radial migration assays at both high (13.2 mg/ml; 18 SZ and 13 control neurospheres) and low (0.05 mg/ml; 27 SZ and 17 control neurospheres) matrigel conditions, SZ neurospheres still migrated less than controls (**SI Fig. 5B**). When we repeated transient miR-9 knockdown using precisely their methodology, using high Matrigel concentrations and measuring average migration of the five furthest migrating cells via NIH ImageJ in both control (90 scrambled and 93 miR-9-knockdown) and SZ (85 scrambled and 87 miR-9-knockdown) neurospheres, we also observed significantly increased migration of control neurospheres ($p<0.00005$), an effect not detected in SZ neurospheres ($p<0.95$) (**SI Fig. 5C**). We speculate that the mode of migration is different in high matrigel "3D" conditions. These technical inconsistencies may reflect the pleiotrophy of miR-9 during neurogenesis (Delaloy et al., 2010; Leucht et al., 2008; Shibata et al., 2008; Shibata et al., 2011; Tan et al., 2012; Zhao et al., 2009), where different patterns of gene expression can lead to unique effects when manipulating miR-9 levels.

*NPC cell viability*

Cell viability assay (Roche) measures absorbance resulting from the reduction of WST-1 to a water-soluble formazan dye in living cells.

*Protein isolation and Western blot analysis*

Cells were isolated, suspended in 1× RIPA lyses buffer (Sigma) supplemented with 1 cOmplete Protease Inhibitor tablet per 50mL and 1 phosSTOP phosphatase inhibitor table per 10mL (Roche), sonicated and centrifuged at 10,000 × g for 10 min at 4°C. 20μg of total protein was separated on a pre-cast 4-20% SDS-polyacrylamide gel(Bio-Rad), transferred to a nitrocellulose membrane and probed with a primary antibody against β-catenin (1:10,000; Millipore), GSK3β (1:5,000; Zymed) or β-actin (1:10,000; Ambion), followed by alkaline-phosphatase-conjugated secondary antibody (1:5,000; Promega), and then visualized using 1 step NBT/BCIP (Thermo Scientific). Western blots were repeated twice using independent protein lysates.

*LC MS/MS quantitative mass spectrometry*

To compare global protein levels in control and SZ NPCs (stably transduced with RV-GFP or RV-miR-9-GFP), we used quantitative label free LC-MS/MS analysis. We injected 2μg of protein from each control (one NPC line each derived from six controls) and SZ (two NPC lines each derived from four SZ patients) hiPSC forebrain NPC line, in triplicate, on a Thermo Q-Exactive mass spectrometer equipped with a Dionex Ultimate 3000 (RSLCnano) chromatography system. Peptides were separated using a 60-minute reverse phase gradient at a flow rate of 250 nL/min. Survey full-scan MS spectra (300–1600 Da) were

acquired in the Q-Exactive with a resolution of 70,000, and the 12 most intense ions from the preview scan were selected for HCD (English et al., 2013). The average MS1 peak width was between 15s and 30s, and the scan time ranged between 1 and 1.5 s, where at least 15 data points were acquired per peak for quantitation. Label-Free Quantification (LFQ) was performed with Max Quant (V1.3.0.2) as described (English et al., 2013; Hubner et al., 2010). Protein and peptide FDR's were set to 0.01, and only proteins with at least two peptides (one uniquely assignable to the protein) were considered as reliably identified. Technical triplicates were run and analyzed for each NPC line; data were successfully extracted from 87 of the 90 samples. LFQ intensity values were used for protein quantification between groups. Statistical analysis was performed in Perseus (V 1.3.0.4), whereby the data was log2 transformed to eliminate distributional skew and improve the normal approximation for validity of p-values. Data imputation was used to replace missing values by values form the normal distribution, and data normalisation was performed by subtracting the median LFQ intensity per case. Student's t-test was then applied to identify proteins differentially expressed between groups at a 5% threshold, and a permutation-based FDR was applied at a 5% threshold. The Database for Annotation, Visualization and Integrated Discovery (DAVID v6.7; http://david.abcc.ncifcrf.gov/) was applied to statistically significant proteins in order to identify enriched biological themes.

**SI REFERENCES**


Bonev, B., Stanley, P., and Papalopulu, N. (2012). MicroRNA-9 Modulates Hes1 ultradian oscillations by forming a double-negative feedback loop. Cell reports *2*, 10-18.

Brennand, K., Savas, J.N., Kim, Y., Tran, N., Simone, A., Hashimoto-Torii, K., Beaumont, K.G., Kim, H.J., Topol, A., Ladran, I.*, et al.* (2015). Phenotypic differences in hiPSC NPCs derived from patients with schizophrenia. Mol Psychiatry *20*, 361-368.

Brennand, K.J., Simone, A., Jou, J., Gelboin-Burkhart, C., Tran, N., Sangar, S., Li, Y., Mu, Y., Chen, G., Yu, D.*, et al.* (2011). Modelling schizophrenia using human induced pluripotent stem cells. Nature.

Chambers, S.M., Fasano, C.A., Papapetrou, E.P., Tomishima, M., Sadelain, M., and Studer, L. (2009). Highly efficient neural conversion of human ES and iPS cells by dual inhibition of SMAD signaling. Nat Biotechnol *27*, 275-280.

Creighton, C.J., Nagaraja, A.K., Hanash, S.M., Matzuk, M.M., and Gunaratne, P.H. (2008). A bioinformatics tool for linking gene expression profiling results with public databases of microRNA target predictions. Rna *14*, 2290-2296.

de Leeuw, C.A., Mooij, J.M., Heskes, T., and Posthuma, D. (2015). MAGMA: generalized gene-set analysis of GWAS data. PLoS Comput Biol *11*, e1004219.

Delaloy, C., Liu, L., Lee, J.A., Su, H., Shen, F., Yang, G.Y., Young, W.L., Ivey, K.N., and Gao, F.B. (2010). MicroRNA-9 coordinates proliferation and migration of human embryonic stem cell-derived neural progenitors. Cell Stem Cell *6*, 323-335.

Eckstrand, K., Addington, A.M., Stromberg, T., Merriman, B., Miller, R., Gochman, P., Long, R., Dutra, A., Chen, Z., Meltzer, P.*, et al.* (2008). Sex chromosome anomalies in childhood onset schizophrenia: an update. Mol Psychiatry *13*, 910-911.

English, J.A., Harauma, A., Focking, M., Wynne, K., Scaife, C., Cagney, G., Moriguchi, T., and Cotter, D.R. (2013). Omega-3 fatty acid deficiency disrupts endocytosis, neuritogenesis, and mitochondrial protein pathways in the mouse hippocampus. Front Genet *4*, 208.

Genomes Project, C., Abecasis, G.R., Auton, A., Brooks, L.D., DePristo, M.A., Durbin, R.M., Handsaker, R.E., Kang, H.M., Marth, G.T., and McVean, G.A. (2012). An integrated map of genetic variation from 1,092 human genomes. Nature *491*, 56-65.

Gogtay, N., Giedd, J.N., Lusk, L., Hayashi, K.M., Greenstein, D., Vaituzis, A.C., Nugent, T.F., 3rd, Herman, D.H., Clasen, L.S., Toga, A.W.*, et al.* (2004). Dynamic mapping of human cortical development during childhood through early adulthood. Proc Natl Acad Sci U S A *101*, 8174-8179.

Hubner, N.C., Bird, A.W., Cox, J., Splettstoesser, B., Bandilla, P., Poser, I., Hyman, A., and Mann, M. (2010). Quantitative proteomics combined with BAC TransgeneOmics reveals in vivo protein interactions. J Cell Biol *189*, 739-754.

Lee, I.S., Carvalho, C.M.B., Douvaras, P., Ho, S.M., Hartley, B.J., Zuccherato, L.W., Ladran, I.G., Siegel, A.J., McCarthy, S., Malhotra, D.*, et al.* (2015). Characterization of molecular and cellular phenotypes associated with a heterozygous CNTNAP2 deletion using patient-derived hiPSC neural cells. NPJ Schizophrenia *1*, 15019.

Leucht, C., Stigloher, C., Wizenmann, A., Klafke, R., Folchert, A., and Bally-Cuif, L. (2008). MicroRNA-9 directs late organizer activity of the midbrain-hindbrain boundary. Nat Neurosci *11*, 641-648.

McCarthy, S.E., Makarov, V., Kirov, G., Addington, A.M., McClellan, J., Yoon, S., Perkins, D.O., Dickel, D.E., Kusenda, M., Krastoshevsky, O.*, et al.* (2009). Microduplications of 16p11.2 are associated with schizophrenia. Nat Genet *41*, 1223-1227.

Packer, A.N., Xing, Y., Harper, S.Q., Jones, L., and Davidson, B.L. (2008). The bifunctional microRNA miR-9/miR-9* regulates REST and CoREST and is downregulated in Huntington's disease. J Neurosci *28*, 14341-14346.

Schizophrenia Working Group of the Psychiatric Genomics Consortium (2014). Biological insights from 108 schizophrenia-associated genetic loci. Nature *511*, 421-427.

Selcuklu, S.D., Donoghue, M.T., Rehmet, K., de Souza Gomes, M., Fort, A., Kovvuru, P., Muniyappa, M.K., Kerin, M.J., Enright, A.J., and Spillane, C. (2012). MicroRNA-9 inhibition of cell proliferation and identification of novel miR-9 targets by transcriptome profiling in breast cancer cells. J Biol Chem *287*, 29516-29528.

Senyuk, V., Zhang, Y., Liu, Y., Ming, M., Premanand, K., Zhou, L., Chen, P., Chen, J., Rowley, J.D., Nucifora, G.*, et al.* (2013). Critical role of miR-9 in myelopoiesis and EVI1-induced leukemogenesis. Proc Natl Acad Sci U S A *110*, 5594-5599.

Shaw, P., Sporn, A., Gogtay, N., Overman, G.P., Greenstein, D., Gochman, P., Tossell, J.W., Lenane, M., and Rapoport, J.L. (2006). Childhood-onset schizophrenia: A double-blind, randomized clozapine-olanzapine comparison. Arch Gen Psychiatry *63*, 721-730.

Shibata, M., Kurokawa, D., Nakao, H., Ohmura, T., and Aizawa, S. (2008). MicroRNA-9 modulates Cajal-Retzius cell differentiation by suppressing Foxg1 expression in mouse medial pallium. J Neurosci *28*, 10415-10421.

Shibata, M., Nakao, H., Kiyonari, H., Abe, T., and Aizawa, S. (2011). MicroRNA-9 regulates neurogenesis in mouse telencephalon by targeting multiple transcription factors. J Neurosci *31*, 3407-3422.

Sporn, A., Addington, A., Reiss, A.L., Dean, M., Gogtay, N., Potocnik, U., Greenstein, D., Hallmayer, J., Gochman, P., Lenane, M.*, et al.* (2004). 22q11 deletion syndrome in childhood onset schizophrenia: an update. Mol Psychiatry *9*, 225-226.

Tan, S.L., Ohtsuka, T., Gonzalez, A., and Kageyama, R. (2012). MicroRNA9 regulates neural stem cell differentiation by controlling Hes1 expression dynamics in the developing brain. Genes to cells : devoted to molecular & cellular mechanisms *17*, 952-961.

Topol, A., Tran, N.N., and Brennand, K.J. (2015). A guide to generating and using hiPSC derived NPCs for the study of neurological diseases. Journal of visualized experiments : JoVE, e52495.

Yoo, A.S., Staahl, B.T., Chen, L., and Crabtree, G.R. (2009). MicroRNA-mediated switching of chromatin-remodelling complexes in neural development. Nature *460*, 642-646.

Yu, T., Liu, K., Wu, Y., Fan, J., Chen, J., Li, C., Yang, Q., and Wang, Z. (2014). MicroRNA-9 inhibits the proliferation of oral squamous cell carcinoma cells by suppressing expression of CXCR4 via the Wnt/beta-catenin signaling pathway. Oncogene *33*, 5017-5027.

Zhang, B., and Horvath, S. (2005). A general framework for weighted gene co-expression network analysis. Stat Appl Genet Mol Biol *4*, Article17.

Zhao, C., Sun, G., Li, S., and Shi, Y. (2009). A feedback regulatory loop involving microRNA-9 and nuclear receptor TLX in neural stem cell fate determination. Nat Struct Mol Biol *16*, 365-371.

Zheng, L., Qi, T., Yang, D., Qi, M., Li, D., Xiang, X., Huang, K., and Tong, Q. (2013). microRNA-9 suppresses the proliferation, invasion and metastasis of gastric cancer cells through targeting cyclin D1 and Ets1. PLoS One *8*, e55719.